Arch. Metall. Mater. **69** (2024), 3, 997-1003

DOI: https://doi.org/10.24425/amm.2024.150920

M.S. MOHSENZADEH[1*]

JUSTIFICATION OF THE CHANGES IN WORK HARDENING EXPONENT BASED ON MICRO-MECHANISMS OF DEFORMATION IN A PLAIN CARBON STEEL

Although several studies have been conducted on the evaluation of work hardening behavior of dual-phase steels with the Hollomon equation, few studies have investigated the factors affecting the number of work hardening stages and the changes of work hardening exponent. Therefore, the aim of this study is to provide a deeper understanding of the deformation micro-mechanisms affecting the work hardening exponent and work hardening behavior in terms of Hollomon equation. For this purpose, samples with microstructures of ferrite-cementite, ferrite-cementite-martensite and ferrite-martensite were produced using appropriate thermomechanical treatments and then subjected to tensile tests. The changes in the work hardening exponent of different microstructures were explained by using the results obtained from the microstructure based modeling of the deformation behavior of the samples. The rate of storage of dislocation loops around particles was suggested as the most important factor influencing the changes in work hardening exponent.

Keywords: Work hardening exponent; Deformation micro-mechanisms; Martensite; Cementite; Bimodal particle size distribution

1. Introduction

Among the various equations available to investigate the work hardening behavior [1-6], it has been proven in the literature that the Hollomon equation is suitable for describing the work hardening behavior of dual-phase steels (DPS) [7-9]. The Hollomon equation is as follows [10]:

$$\sigma = K\varepsilon^n \tag{1}$$

Where σ is the true stress, ε is the true strain, n is work hardening exponent and K is strength coefficient. Taking the logarithm from both sides of the equation, it is obtained:

$$\ln\sigma = \ln K + n\ln\varepsilon \tag{2}$$

The Hollomon equation parameters, i.e. work hardening exponent (n) and strength coefficient (K), could be determined using the slope and the intercept to the ordinate axis of the fitted line to the stress-strain curves in double logarithmic scale, i.e. $\ln\sigma$-$\ln\varepsilon$ curves, respectively.

In a number of researches about the analysis of the work hardening behavior of DPS with the Hollomon equation, two-stage work hardening behavior has been observed for different volume fractions of martensite [11-13]. The two-stage work hardening behavior is attributed to the deformation of ferrite in the first stage and the co-deformation of ferrite and martensite in the second stage [11]. It was proved that by increasing the volume fraction of martensite from 28% to 50%, the work hardening exponent of the first stage increased, while the work hardening exponent of the second stage and the transition strain between the two stages decreased [11]. Also, for a certain volume fraction of martensite, the work hardening exponent of the first stage was significantly lower than the work hardening exponent of the second stage [11].

Other studies have predicted one-stage or two-stage work hardening behavior for DPS in terms of the Hollomon equation, depending on the volume fraction of martensite [11,14,15]. In DPS containing a volume fraction of martensite less than 50%, one-stage work hardening occurred, and in a volume fraction greater than 50%, two-stage hardening occurred [11,14]. In another research, the change of one-stage to two-stage work hardening behavior was observed in the martensite volume fraction of 36% [15]. In addition, it has been reported that the increase in the martensite volume fraction leads to an increase in the work hardening exponent [14,15]. In this group of researches

[1] UNIVERSITY OF GONABAD, DEPARTMENT OF MATERIALS AND METALLURGICAL ENGINEERING, GONABAD, IRAN

* Corresponding author: mmohsenzaadeh@gmail.com

[11,14,15], unlike the previous group [11,13], in the case of two-stage work hardening, the work hardening exponent of the first stage is significantly higher than the second stage.

A review of research that predicts the two-stage work hardening behavior for DPS with any volume fraction of martensite [11,13], shows that there is a clear yield point in the stress-strain curve and yielding is not completely continuous. Besides, the initial work hardening rate is not as high as it is typical in DPS. On the other hand, in studies that have observed two types of work hardening behavior [11,14,15], for each volume fraction of martensite, completely continuous yielding and high initial work hardening rates occur. This can be attributed to the strength of the ferrite matrix [16]. In the first group, the strength of the ferrite matrix is such that it prevents continuous yielding and creates a clear yield point in the stress-strain curve. But in the second group, the strength of the ferrite matrix does not prevent the continuous yielding of DPS, and the initial work hardening rate is high.

Investigating the work hardening of ultra-fine-grained DPS with a martensite volume fraction of more than 50% with the Hollomon equation showed that two-stage work hardening occurs in these steels [18]. The work hardening exponent in the first stage was somewhat lower than in the second stage. In the deformation behavior of these steels, continuous yielding and high initial work hardening rate, which is common in dual-phase steel, were observed. Soliman et al. [8] investigated the effect of martensite morphology and volume fraction as well as ferrite grain size on the work hardening behavior of DPS. The results of this study showed that the volume fraction of martensite has the greatest effect on the work hardening exponent in the first stage. The mean free path in ferrite was considered as an important microstructural factor affecting the work hardening exponent in the first stage.

Although several studies have been conducted on the evaluation of DPS work hardening behavior with the Hollomon equation, few studies have investigated the origin of the two-stage and one-stage work hardening behavior as well as the factors affecting the changes of work hardening exponent. Therefore, the aim of this study is to provide a deeper understanding of the deformation micro-mechanisms affecting the work hardening exponent and to justify the observed work hardening behavior in terms of Hollomon equation.

2. Materials and methods

Low-carbon steel sheet with a thickness of 4.6 mm was used to produce the desired microstructures. The chemical composition of this steel sheet was Fe-0.16 C-0.41 Si-1.15 Mn-0.018 P-0.01 S (wt.%). Samples with three different types of microstructures including ferrite-cementite, ferrite-cementite-martensite, and ferrite-martensite were produced. The production steps of steel with ferrite-cementite microstructure include austenitizing samples of steel sheet with dimensions of 15×80 mm at 1000°C for 30 minutes in a laboratory box furnace, quenching in ice brine solution in order to produce a completely martensitic structure, tempering the resulting martensitic structure for 1 hour at 650°C in order to make the produced samples easier to roll, 80% cold rolling of the tempered martensite samples, and finally heating of the cold rolled sample for 2 hours at 650°C. Rolling was done in such a way that during each rolling pass, about 0.5 mm of thickness reduction was created in the sample. In order to produce steels with ferrite-cementite-martensite and ferrite-martensite microstructure, samples of the initial sheet after going through the previous steps were finally tempered for 1 hour and intercritically annealed at 740°C for 1 minute and 15 minutes followed by quenching in ice brine solution. The sample with a ferrite-cementite microstructure that included fine cementite particles was named as FC sample, the sample with a ferrite-cementite-martensite microstructure that included fine cementite particles and coarse martensite particles was named as FCM sample, and the sample with ferrite-martensite microstructure that included coarse martensite particles was named as FM sample.

The microstructure of the samples was examined with an Olympus BX60M optical microscope and a Leo 1450VP scanning electron microscope (SEM). The preparation of the samples for microstructural investigations included mounting, grinding, polishing, and etching with 2% Nital solution. The volume fraction of cementite phase and martensite phase, and the size of martensite islands and cementite particles, as well as the ferrite grain size in each sample were determined using Clemex image analysis software on at least 10 SEM micrographs.

The stress-strain (σ-ε) curves of the produced steels with different microstructures were obtained using tensile tests. Besides, the stress-strain curve of steel containing 0.09 wt.% carbon, which can be considered as the stress-strain curve of ferritic steel [17], were obtained for comparison. These tests were performed on the tensile samples produced according to the ASTM-E8 standard, with strain rate of 0.002 s^{-1} by Zwick Z250 universal tensile test machine. Using the obtained data, the stress-strain curves were plotted in double logarithmic scale ($\ln\sigma$-$\ln\varepsilon$ curves). Lines were fitted to the $\ln\sigma$-$\ln\varepsilon$ curves and the equations of the fitted lines were obtained. The Hollomon equation parameters, i.e. work hardening exponent (n) and strength coefficient (K), were determined using the slope and the intercept to the ordinate axis of the fitted line, respectively.

3. Results and discussion

3.1. Examination of the microstructures of the samples

Fig. 1a shows the microstructure of the martensitic steel produced as a result of the quenching of the steel sheet after 30 minutes austenitizing at 1000°C. Lath martensite, which is common in low carbon steels, can be seen in the micrograph. The microstructure consists of a fine morphology of martensite packets and blocks. The SEM micrograph of the microstructure of martensite tempered for 1 hour at 650°C is shown in Fig. 1b. Ferrite grains and spherical cementite particles, which are mainly located in the grain boundaries, can be seen in the micrograph.

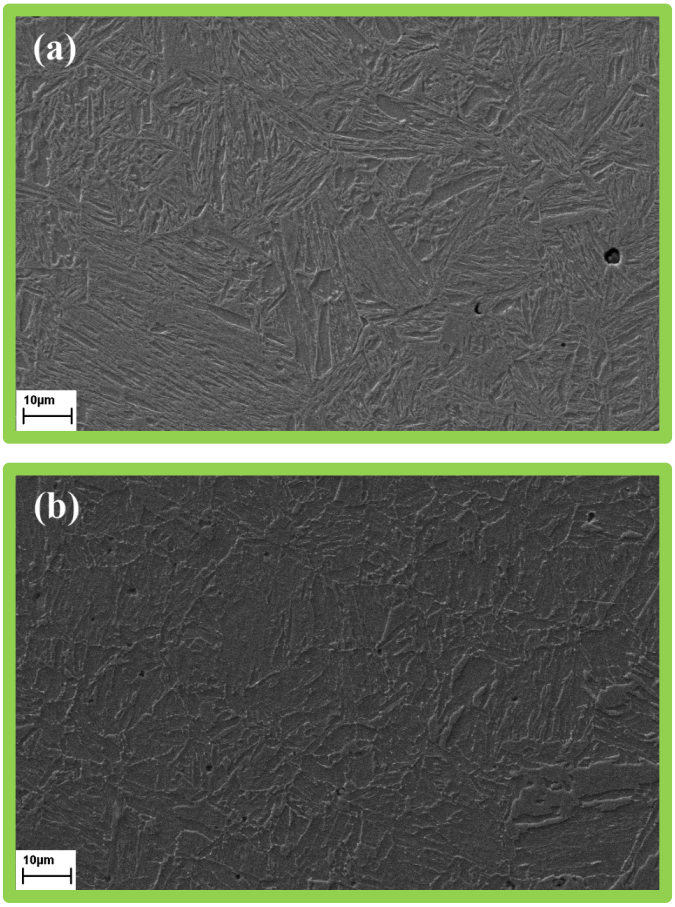

Fig. 1. The microstructures of, a) the martensitic sample, and b) the martensite sample after tempering for 1 hour at 650°C

The microstructure of the sample FC is shown in Fig. 2a. Based on the results of quantitative metallography, in this sample, a uniform distribution of cementite particles with an average size of 150 nm and a volume fraction of 3.2% has been produced in a matrix of ferrite with an average grain size of 10 µm. Using the gray threshold toolbox in Clemex software, it is possible to separate the phases in the SEM micrograph based on the gray level. Due to the fact that the cementite particles appear brighter than the background in the SEM micrograph, they were separated from the matrix using this tool and marked with red color. Because the grain boundaries also appear brighter than the matrix in the SEM micrograph, they were selected along with the cementite particles. For this reason, all the selected parts except the cementite particles were deleted with the eraser tool. Finally, the area percent of red areas compared to the field was calculated using Clemex software and was considered as the volume fraction of cementite particles. Due to the fact that the studied samples were plain carbon steels, its alloying elements were not to the extent that other alloy carbides were formed at the temperature of the tempering treatment [19].

Fig. 2b shows the microstructure of the sample FCM. After 1 minute of inter-critical annealing, 13% of martensite islands with an average size of 2.25 µm are formed in the microstructure. In the ferrite-cementite microstructure, the interface between the cementite particles and the ferrite grain boundaries are the most suitable places for austenite nucleation during intercritical annealing [7]. Therefore, martensite islands are mainly formed in ferrite grain boundaries. As can be seen in the SEM micrograph (Fig. 2b), only a certain percentage of cementite particles are dissolved in austenite (martensite after quenching), and 1.2% of cementite particles remain in the microstructure. Due to the higher dissolution of carbon in austenite compared to ferrite, austenite (martensite at room temperature) forms in carbon-rich places of the microstructure. The conditions of austenite nucleation (i.e., nucleation in carbon-rich regions and high-energy non-equilibrium defects) exist for cementite particles located at the boundaries of ferrite grains. Therefore, the interface between

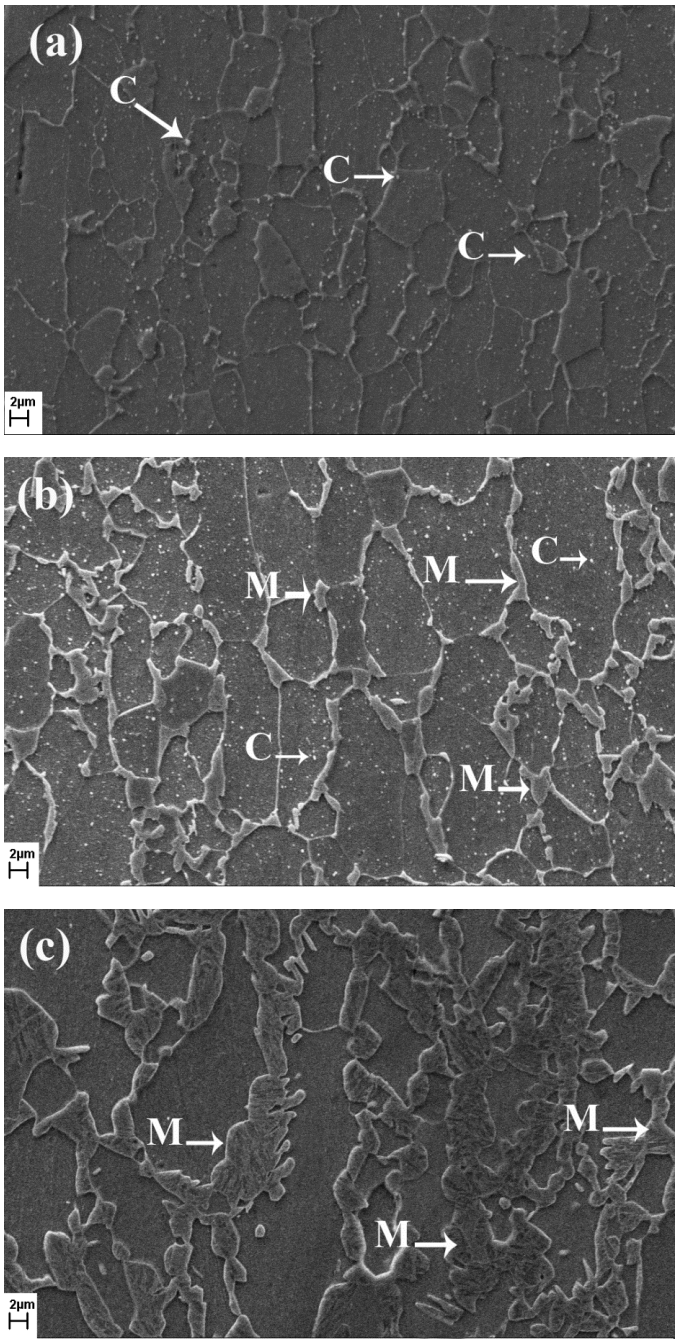

Fig. 2. SEM micrographs, a) sample FC (ferrite-2.3% cementite), b) sample FCM (ferrite-1.2% cementite-13% martensite) and c) sample FM (ferrite- 40% martensite). C: cementite, M: martensite

cementite particles and ferrite grain boundaries are the preferred places for austenite nucleation in ferrite-cementite microstructures [20]. As previous studies in the field of austenite formation have shown, the formation of austenite at the interface between the cementite particles located inside the grain and the ferrite matrix is significantly delayed, until the cementite particles are mainly dissolved without austenite nucleation. The carbon of the particles diffuses towards the growing austenite islands along the grain boundaries [20]. In some cases, the formation of austenite islands at the cementite particles located inside the grain has been reported to a lesser extent compared to the particles located at the grain boundaries [20]. The method of calculating the volume fraction of cementite particles in the sample FCM was similar to the sample FC. In order to calculate the volume fraction of martensite islands, the boundaries of martensite islands were marked with a pencil tool and the islands were filled with blue color. Finally, the volume fraction of the blue areas compared to the matrix was calculated using Clemex software.

After 15 minutes of intercritical annealing, 40% of martensite islands with an average size of 4.15 μm were formed in the microstructure of the FM sample (Fig. 2c). Cementite particles are not observed in the microstructure of this sample, which shows that all cementite particles have transformed during this period. Because the martensite phase is harder than ferrite, it is less affected by etchant and corrodes less. For this reason, in the SEM micrographs prepared using secondary electrons, martensite appears slightly more prominent than ferrite. In addition, due to its lath structure, the martensite surface has ridges and depressions after etching and is not smooth. This is clear in the SEM micrographs (especially Fig. 2c clearly shows this). But the ferrite surface is completely smooth. The average grain size of ferrite in samples FCM and FM is 10 μm. As a result, it can be said that significant grain growth did not occur during the intercritical annealing treatment.

3.2. Evaluation of work hardening behavior in terms of Hollomon equation

The plots of the logarithm of stress ($\ln\sigma$) in terms of the logarithm of strain ($\ln\varepsilon$) for the studied samples and ferritic steel are shown in Figs. 3a to 3d. According to the changes of $\ln\sigma$ with $\ln\varepsilon$, three stage work hardening behavior for the sample FCM (Fig. 3c) and two-stage work hardening behavior for samples FC, FM and ferritic steel (Figs. 3a, b, and d) can be seen in terms of the Hollomon equation. The lines fitted to the stress-strain curves in double logarithmic scale (the $\ln\sigma$-$\ln\varepsilon$ plots) at each stage of the work hardening and the equation of the lines are shown in Fig. 3. Work hardening exponent (n) and strength coefficient (K) for each stage of work hardening of the samples are given in TABLE 1. The considered criterion for linear fitting to the $\ln\sigma$-$\ln\varepsilon$ plots was to fit the minimum number of lines so that the least square regression factor (R^2) values of the lines are greater than or equal to 0.99. Based on this, two-stage work hardening behavior (with two values of n and K) or three-stage

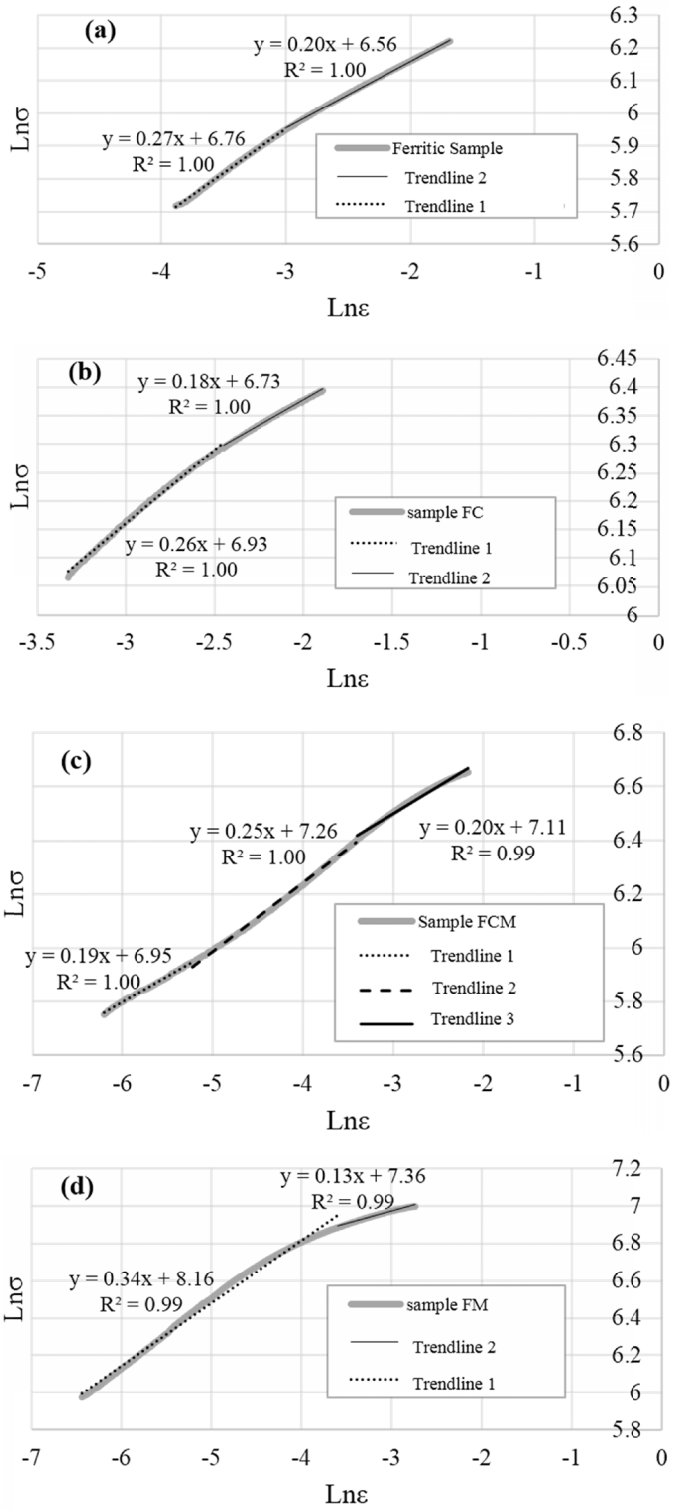

Fig. 3. $\ln\sigma$ plotted versus $\ln\varepsilon$, and the fitted lines to the graphs for the studied samples

work hardening behavior (with three value of n and K) were obtained for the studied samples (TABLE 1).

According to the data in TABLE 1, it can be seen that in samples with two-stage work hardening behavior (the sample FC and FM), the values of n and K in the first work hardening stage are higher than the second stage. For the sample FCM, in a very small range of strain at the beginning of the deformation (from

TABLE 1

The values of work hardening exponent (n) and strength coefficient (K) for the samples

Samples	n			K (MPa)		
Ferritic sample	$n_1 = 0.27$	$n_2 = 0.2$ ($\varepsilon_{tr}^{*} = 0.03$, $\varepsilon_{total}^{**} = 0.17$)		$K_1 = 862.64$	$K_2 = 706.27$	
FC	$n_1 = 0.26$	$n_2 = 0.18$ ($\varepsilon_{tr} = 0.05$, $\varepsilon_{total} = 0.12$)		$K_1 = 1022.49$	$K_2 = 837.14$	
FCM	$n_1 = 0.19$	$n_2 = 0.25$ ($\varepsilon_{tr} = 0.003$)	$n_3 = 0.2$ ($\varepsilon_{tr} = 0.03$, $\varepsilon_{total} = 0.11$)	$K_1 = 1043.15$	$K_2 = 1422.26$	$K_3 = 1224.15$
FM	$n_1 = 0.34$	$n_2 = 0.13$ ($\varepsilon_{tr} = 0.025$, $\varepsilon_{total} = 0.063$)		$K_1 = 3498.19$	$K_2 = 1571.84$	

* The transition strain between the work hardening stages.
** The total plastic strain.

plastic strain of zero to plastic strain of about 0.003), the slope of the graph and as a result the value of n_1 is low ($n_1 = 0.19$) and then increases in the second stage of work hardening ($n_2 = 0.25$). After plastic strain of about 0.03, the work hardening exponent decreases ($n_3 = 0.2$). The values of n_1 of the sample containing fine cementite particles (sample FC) and the sample containing coarse martensite particles (sample FM) are greater than the values of n of the sample containing bimodal-sized particles (sample FCM). In the second stage of work hardening, the values of n_2 of the samples FC and FM are reduced compared to the values of n of the sample FCM. The change of work hardening exponent in these samples can be explained according to the micro-mechanisms of deformation. Work hardening exponent (n) depends on the ability to accumulate dislocations in the microstructure [23]. The higher the dislocation accumulation ability in the microstructure, the higher the value of n. In an annealed steel, because the ability to accumulate dislocations and thus the tendency to work harden is high, the value of n is high. If the dislocation accumulation ability decreases and dislocation saturation occurs, the value of n will decrease. In the previous article, a microstructure based model was developed that well described the deformation behavior of samples with microstructures including fine particles, coarse particles, and particles with bimodal grain size distribution [22]. In this model, the contribution of statistically stored dislocations (SSDs), geometrically necessary dislocations (GNDs) and Orowan dislocation loops stored around particles to isotropic work hardening were considered. Kinematic work hardening was calculated by considering the contribution of second phase particles based on the Eshelby approach. The deformation behavior of samples FC, FM and FCM was modeled using the microstructure based model developed in the previous article. After modeling, the evolution of the number of Orowan dislocation loops stored around a second phase particle (N) with plastic strain (ε_p) and the maximum number of stored dislocation loops around a second phase particle (N^*) were determined using the theoretical model. The reader can refer to the previous article to know the details of the modeling [22]. Fig. 4 shows the fraction of places available to store dislocations around particles occupied by dislocation loops (N/N^*) as a function of plastic strain (ε_p). This parameter is a good indicator of the work hardening capacity, and it justifies the observed trend in the changes of the work hardening exponents of the samples. The greater the fraction of sites occupied for a given strain, the greater the work hardening capacity and the greater the n. In addition, if N/N^* increases rapidly and tends to 1, n decreases due to the reduction of dislocation accumulation ability and dislocation saturation. According to Fig. 4, it can be concluded that in the early stages of deformation, the rate of accumulation of dislocation loops around coarse martensite particles in the sample FM is the highest. In addition, the sample FC has a faster rate of dislocation loops accumulation than the sample FCM. Therefore, due to the greater ability to accumulate dislocations in the early stages of deformation, n_1 in samples FM and FC (equal to 0.34 and 0.26, respectively) is higher than n values in the sample FCM (equal to 0.24). In the sample FCM, due to the presence of bimodal-sized particles, the contribution of moving dislocations reaching the particles is less than if there is only one type of particle. For this reason, the ability to accumulate dislocation loops and the rate of increase of N/N^* are lower.

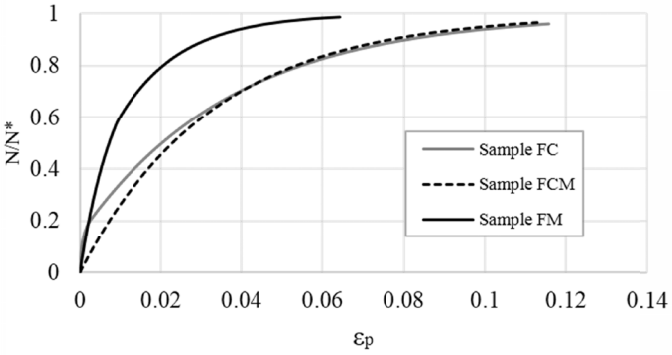

Fig. 4. The plots of the fraction of places around particles occupied by dislocation loops (N/N^*) as a function of plastic strain (ε_p)

In samples FC and FM, because the rate of increase of N/N^* in initial strains is high, work hardening is two-stage. Due to the high rate of dislocation accumulation in the early stages of deformation, the ability to accumulate dislocations decreases in the later stages of deformation and leads to a decrease in n. In the three-phase sample (the sample FCM), work hardening mechanisms include isotropic hardening (caused by GNDs stored around cementite particles and martensite islands, GNDs stored at the boundaries of ferrite grains, and statistically stored dislocations (SSDs)) and kinematic hardening (caused by the internal stress due to the mismatch of the shape of the particle and its corresponding cavity) created by cementite particles and martensite islands [22,24]. In the early stages of deformation, the density of free dislocations is limited and these dislocations are

distributed between two types of particles (cementite particles and martensite islands). Therefore, the dislocation accumulation ability and work hardening ability (n_1 value) are low. Gradually more dislocations are produced during plastic deformation and work hardening ability (n_2 value) increases. In the case of samples containing one type of particle, this trend is not observed (Figs. 2b and 2d). In the final stages of deformation, due to the reduction of places available to store dislocations, the work hardening ability (n_3 value) decreases. Because dislocation accumulation occurs at a slower rate in the sample FCM, its dislocation accumulation capacity decreases less than the samples FC and FM . As a result, the amount of reduction in work hardening exponent in the sample FCM (from n_2 = 0.25 to n_3 = 0.2) is lower than the samples FC and FM (from n_1 = 0.26 to n_2 = 0.18, and from n_1 = 0.34 to n_2 = 0.13, respectively). According to the data reported in TABLE 1, it can be seen that the value of n_2 in the sample FM is lower than that of the sample FC. This can be attributed to the lower work hardening ability of the sample FM than the sample FC in the second stage of work hardening. The accumulation of more dislocations and the increase in the strength of the ferrite matrix due to the work hardening of the matrix caused the mobility of dislocations to decrease in the sample FM compared to the sample FC.

In a number of studies, two-stage hardening has been observed for DPS [11,14,15,23]. Mainly, the two-stage work hardening behavior has been attributed to the deformation of ferrite in the first stage and the simultaneous deformation of ferrite and martensite in the second stage. The martensite phase in the FM sample did not undergo plastic deformation. But the FM sample had a two-stage hardening behavior. In this study, it was found that another reason caused the two-stage work hardening.

Fig. 5 shows the plots of the density of statistically stored dislocations (SSDs) and geometrically necessary dislocations (GNDs) as a function of plastic strain for samples FC, FM and FCM. It should be noted that the ferrite grain size is the same in all samples. As can be seen, the density of SSDs and GNDs is the same at each stage of deformation for these samples. Therefore, it can be concluded that the accumulation capacity of SSDs and GNDs is the same for the samples, and the statistically stored dislocations and geometrically necessary dislocations have no role in the observed changes in the work hardening exponents of the samples FC, FM, and FCM. In addition, the kinematic work hardening (caused by the back stress created by the accumulation of dislocations) does not affect the work hardening exponent. Kinematic work hardening depends on the particle size and its volume fraction [22]. Therefore, the sample FM with the highest volume fraction of coarse martensite particles has the highest kinematic work hardening value. The kinematic work hardening in the sample FCM is reduced compared to the sample FM and reaches the lowest value in the sample FC. But the trend of changes in work hardening exponent is different (See TABLE 1). Although having a lower kinematic work hardening than the sample FCM, the sample FC has more work hardening exponent than the sample FCM in the first stage of work hardening.

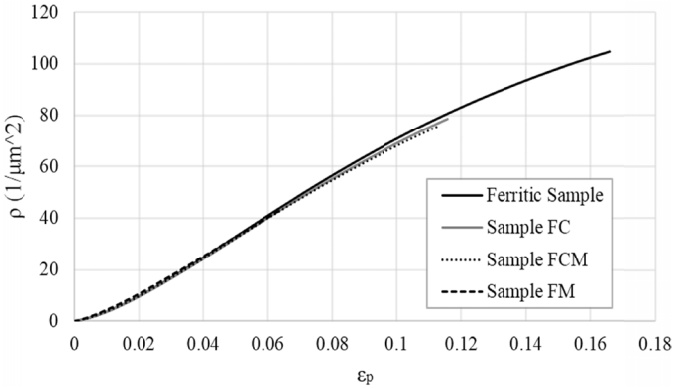

Fig. 5. The plots of the density of statistically stored dislocations (SSDs) and geometrically necessary dislocations (GNDs) as a function of plastic strain for the samples

Two-stage work hardening is also observed in the ferritic sample. The n_1 value of the ferritic sample is higher than that of the samples FC and FCM (TABLE 1). Since the ferrite in the ferritic sample is work hardened to a lesser extent than other samples, the strength of ferrite is less. As a result, the mobility of dislocations is higher and the work hardening ability and the value of the work hardening exponent are also higher in the early stages of deformation than the samples FC and FCM. But after a small amount of plastic strain (0.03), the places available for the accumulation of dislocations are quickly occupied in the ferritic sample and the work hardening exponent decreases. Despite this, the n_2 value of the ferritic sample (0.2) is higher than the n_2 of the samples FC and FM (0.18 and 0.13, respectively). Because the ferrite in the ferritic sample is work hardened to a lesser extent than the ferrite matrix of the samples FC and FM, the mobility of dislocations is higher in the former than the latter.

Fig. 6 shows the difference between the true stress in the maximum load and the yield stress (σ_u-σ_y) for the studied samples. This parameter can be considered as a measure of work hardening [9]. As can be seen, the work hardening is the lowest in the ferritic sample and gradually increases in the samples FC and FCM and reaches the maximum value in the sample FM. By comparing the trend observed in the work hardening of the samples (Fig. 6) with the trend of changes in the work harden-

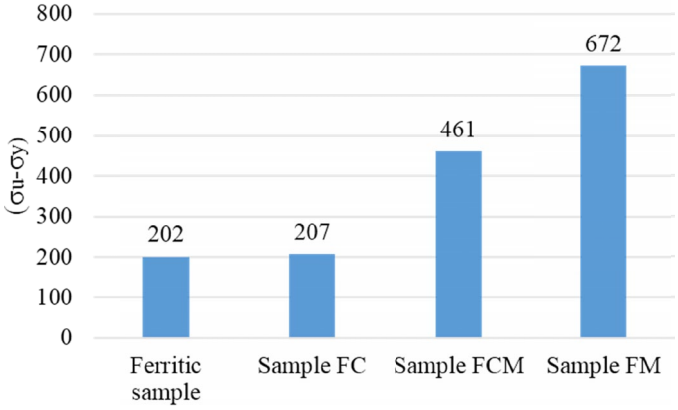

Fig. 6. The plot of the difference between the true stress in the maximum load and the yield stress (σ_u-σ_y) for the studied samples

ing exponents (TABLE 1), one may conclude that the work hardening exponent cannot be considered as a measure of work hardening. In fact, work hardening depends on the density of dislocations, while the work hardening exponent does not depend on the density of dislocations. Despite having a lower density of dislocation loops than the sample FCM, the sample FC has a higher n_1 value. On the other hand, the changes in the strength coefficients of the samples well reflect the trend of changes in the work hardening. The value of the strength coefficient in the first stage of deformation is the lowest value in the ferritic sample, it increases in the samples FC and FCM, and reaches the highest value in the sample FM. There is a similar trend of change for the strength coefficient values in the second stage of deformation.

4. Conclusions

The purpose of this study was to investigate the work hardening behavior of steel samples with different microstructures according to the Hollomon equation, and to analyze the changes in the work hardening exponent based on the deformation micromechanisms. The main results can be summarized as follows:

- The samples containing one type of particle (cementite or martensite) showed a two-stage work hardening behavior, while the sample containing two types of particles (cementite and martensite) had a three-stage work hardening behavior.
- The work hardening exponents of the samples depend on the ability to accumulate dislocations around the particles. In the sample containing cementite and martensite particles, due to the presence of particles with bimodal size distribution, the contribution of moving dislocations reaching the particles is less than if there is only one type of particle. For this reason, in the early stages of deformation, the rate of accumulation of dislocation loops around the particles and as a result, the work hardening exponent in the sample containing two types of particles is lower than the samples containing one type of particle.
- In the next stages of deformation, the ability to accumulate dislocations in the samples containing one type of particle is reduced due to the high rate of dislocation accumulation in the previous stage, and it leads to a decrease in the work hardening exponent, while in the sample containing two types of particles due to the more gradual accumulation of dislocations, the decrease of the work hardening exponent is lower.
- Based on the obtained results, it was determined that the work hardening exponent is only dependent on the work hardening ability and does not depend on the density of dislocations and the back stress created by the accumulation of dislocations. In addition, the work hardening exponent cannot be considered as a measure of work hardening. But the strength coefficients reflect the changes of work hardening in the samples well.

REFERENCES

[1] S.K. Gupta, R. Manna, K. Chattopadhyay, Materials Science and Engineering: A **860**, 144318 (2022).

[2] P. Ludwik, Elemente der technologischen Mechanik, Springer, (1909).

[3] J.V. Fernandes, D.M. Rodrigues, L.F. Menezes, M.F. Vieira, International Journal of Plasticity **14**, 537-550 (1998).

[4] D.C. Ludwigson, Metallurgical Transactions A **2**, 2825-2828 (1971).

[5] E. Voce, Metallurgia **51**, 219-226 (1955).

[6] P.V. Sivaprasad, S. Venugopal, S. Venkadesan, Metallurgical and Materials Transactions A **28**, 171-178 (1997).

[7] H. Mirzadeh, M. Alibeyki, M. Najafi, Metallurgical and Materials Transactions A **48**, 4565-4573 (2017).

[8] M. Soliman, H. Palkowski, Steel Research International **92**, 2000518 (2021).

[9] A. Zare, A. Ekrami, Materials Science and Engineering: A **528**, 4422-4426 (2011).

[10] J.H. Hollomon, Trans Metall Society of AIME **162**, 268-290 (1945).

[11] H. Ashrafi, M. Shamanian, R. Emadi, N. Saeidi, Transactions of the Indian Institute of Metals **70**, 1575-1584 (2017).

[12] X. Luo, Z. Mi, Y. Wu, Y. Yang, H. Jiang, K. Hu, Metals **12**, 1026 (2022).

[13] Y. Mazaheri, A. Kermanpur, A. Najafizadeh, Metallurgical and Materials Transactions A **46**, 3052-3062 (2015).

[14] O. Abedini, M. Behroozi, P. Marashi, E. Ranjbarnodeh, M. Pouranvari, Materials Research **22** (2019).

[15] S.S.G. Banadkouki, H.R. Pakzaman, International Journal of Materials Research **111**, 983-994 (2020).

[16] M.S. Mohsenzadeh, M. Mazinani, Materials Science and Engineering: A **673**, 193-203 (2016).

[17] T. Gladman, I. McIvor, F. Pickering, Journal of Iron and Steel Institute **210**, 916-930 (1972).

[18] Y. Mazaheri, A.H. Jahanara, M. Sheikhi, A.G. Kalashami, Materials Science and Engineering: A **761**, 138021 (2019).

[19] D.A. Porter, K.E. Easterling, M. Sherif, Phase Transformations in Metals and Alloys, 3rd ed., (Revised Reprint), CRC Press, Boca Raton, (2009).

[20] Q. Lai, M. Gouné, A. Perlade, T. Pardoen, P. Jacques, O. Bouaziz, et al., Metallurgical and Materials Transactions A **47**, 3375-3386 (2016).

[21] W.D. Callister, D.G. Rethwisch, Materials science and engineering: an introduction, Wiley New York, (2018).

[22] M.S. Mohsenzadeh, M. Mazinani, Materials Science and Engineering: A **702**, 113-124 (2017).

[23] P. Movahed, S. Kolahgar, S. Marashi, M. Pouranvari, N. Parvin, Materials Science and Engineering: A **518**, 1-6 (2009).

[24] G. Fribourg, Y. Bréchet, A. Deschamps, A. Simar, Acta Materialia **59**, 3621-3635 (2011).